Single Wall Carbon Nanotubes/Polypyrrole Composite Thin Film Electrodes: Investigation of Interfacial Ion Exchange Behavior

Freddy Escobar-Teran, Hubert Perrot, Ozlem Sel

▶ **To cite this version:**

Freddy Escobar-Teran, Hubert Perrot, Ozlem Sel. Single Wall Carbon Nanotubes/Polypyrrole Composite Thin Film Electrodes: Investigation of Interfacial Ion Exchange Behavior. Journal of Composites Science, 2021, 5 (1), pp.25. 10.3390/jcs5010025 . hal-03222699

HAL Id: hal-03222699

https://hal.sorbonne-universite.fr/hal-03222699

Submitted on 10 May 2021

HAL is a multi-disciplinary open access archive for the deposit and dissemination of scientific research documents, whether they are published or not. The documents may come from teaching and research institutions in France or abroad, or from public or private research centers.

L'archive ouverte pluridisciplinaire **HAL**, est destinée au dépôt et à la diffusion de documents scientifiques de niveau recherche, publiés ou non, émanant des établissements d'enseignement et de recherche français ou étrangers, des laboratoires publics ou privés.

Distributed under a Creative Commons Attribution 4.0 International License

Journal of
Composites Science

MDPI

Article

Single Wall Carbon Nanotubes/Polypyrrole Composite Thin Film Electrodes: Investigation of Interfacial Ion Exchange Behavior

Freddy Escobar-Teran [1,2], Hubert Perrot [1] and Ozlem Sel [1,*]

[1] Laboratoire Interfaces et Systèmes Electrochimiques, LISE, UMR8235, Sorbonne Université, CNRS, F-75005 Paris, France; fescobarteran@hotmail.com (F.E.-T.); hubert.perrot@sorbonne-universite.fr (H.P.)
[2] Facultad de Ingeniería en Sistemas, Electrónica e Industrial, Universidad Técnica de Ambato, Avenida los Chasquis y Río Payamino, Ambato 180103, Ecuador
* Correspondence: ozlem.sel@sorbonne-universite.fr

Abstract: Single-wall carbon nanotubes/polypyrrole (SWCNT/PPy) composite thin-film electrodes were prepared by electrodeposition of the pyrrole monomer on a porous network made of SWCNT bundles. Electrode/electrolyte interface, which is intimately related to the pseudocapacitive charge storage behavior, is investigated by using coupled electrogravimetric methods (electrochemical quartz crystal microbalance (EQCM) and its coupling with electrochemical impedance spectroscopy, *Ac*-electrogravimetry), in a 0.5 M NaCl electrolyte (pH = 7). Our results show that the range of usable potential is greater for composite SWCNT/PPy films than for SWCNT films, which should allow a higher storage capacity to be obtained. This effect is also confirmed by mass variation measurements via EQCM. The mass change (corresponding to the amount of (co)electroadsorbed species) obtained with composite SWCNT/PPy films is four times greater than that observed for pristine SWCNT films if the same potential range is examined. The permselectivity is also greatly improved in the case of composite SWCNT/PPy films compared to SWCNT films; the former shows mainly cation exchange preference. The quantities of anions estimated by *Ac*-electrogravimetric measurements are much lower in the case of composites. This corroborates the better permselectivity of these composite SWCNT/PPy films even with a moderate amount of PPy.

Keywords: carbon/polymer composites; carbon nanotubes; conducting polymers; SWCNT; doped polypyrrole; electrochemical quartz crystal microbalance; EQCM; electrode/electrolyte interface; ion transfer

check for updates

Citation: Escobar-Teran, F.; Perrot, H.; Sel, O. Single Wall Carbon Nanotubes/Polypyrrole Composite Thin Film Electrodes: Investigation of Interfacial Ion Exchange Behavior. *J. Compos. Sci.* **2021**, *5*, 25. https://doi.org/10.3390/jcs5010025

Received: 16 December 2020
Accepted: 11 January 2021
Published: 14 January 2021

Publisher's Note: MDPI stays neutral with regard to jurisdictional claims in published maps and institutional affiliations.

Copyright: © 2021 by the authors. Licensee MDPI, Basel, Switzerland. This article is an open access article distributed under the terms and conditions of the Creative Commons Attribution (CC BY) license (https://creativecommons.org/licenses/by/4.0/).

1. Introduction

Polymers and polymeric composites are a unique class of materials, extensively used in numerous fields of applications such as electrochemical energy storage and conversion [1]. Due to their peculiar physicochemical and mechanical properties, these materials have been stimulating new research that aims at refining their structural, morphological and compositional characteristics to achieve the desired properties required for electrode or electrolyte materials used in energy devices [2,3].

Among them, supercapacitors (SCs) can provide a large amount of power in a relatively short time and can operate for a very high number of charge/discharge cycles and a longer lifetime than batteries [4,5]. These versatile attributes have led to their incorporation in a wide range of applications (such as city transit buses with stop-and-go driving, cranes and forklifts [6]). SC devices consist of two electrodes in contact with an electrolyte electrically isolated by a separator. During the charging process, the charges are stored and separated across the two electrode/electrolyte interfaces, which provides electric energy for the external load upon discharge. Briefly, SCs can be classified into two types with regard to their charge storage mechanism: electrical double-layer capacitors (EDLCs) and

pseudocapacitors. EDLCs store charges by electrostatic adsorption of electrolyte ions at the electrode–electrolyte interface, typically use carbon materials as electrodes [7–9]. As for the pseudocapacitors, energy is stored by fast and reversible redox reactions between the electrolyte and electroactive species on the electrode surface at characteristic potentials, commonly employing transition metal oxides and conducting polymers (CPs) as electrode materials [10,11].

Due to their high conductivity, porosity and superior electrochemical stability, carbon materials are widely used as EDLC electrode materials [12], namely activated carbon (ACs), carbon nanotubes (CNTs) and graphene are the most studied examples. CNTs are of particular interest for the development of SC electrodes since they present unique tubular structures and superior electrical conductivity, mechanical, thermal and chemical stability [7]. CNTs have been considered as a promising candidate for high-power electrode material because of the aforementioned properties. In spite of the fact that the surface area of CNTs (800 $m^2 \cdot g^{-1}$) is small as compared to ACs (2000–3000 $m^2\ g^{-1}$) [7,13], they can offer a reasonable specific capacitance [14], which is speculated to stem from their aligned pore structures, which, therefore, contribute to higher ion diffusion kinetics. Another option is the use of CNTs as support for electroactive materials because of their high mechanical resilience and open tubular network, which can form composite materials with metal oxides and/or CPs [15,16].

Regarding the electrode materials for pseudocapacitors, CPs are a very attractive solution due to their low price, non-toxicity and tunable chemical, electrical and physical properties. These polymers can be electrochemically doped in the presence of an electrolyte to obtain very good electrical conductivity (10 to 100 $S.cm^{-1}$) and a wide electrochemical window. The most commonly used CPs for pseudocapacitive charge storage involve poly(3,4-ethylenedioxythiophene) (PEDOT) [17], polypyrrole (PPy) [18], polyaniline (PANI) [19], and polythiophene (PTh) [20]. Moreover, transitional metal oxides such as ruthenium oxide (RuO_2) [21], MnO_2 [22], ZnO [23], and NiO [24] have also been widely studied. Although the pseudo-capacitance can be much higher than EDL capacitance, it suffers from low-power density and poor stability upon cycling, which further highlights the interest of composite electrodes, uniting their benefits in a single electrode. In this context, a mix of carbon materials and CPs, merging the advantages of the two components, was evaluated in the field of pseudocapacitors. Indeed, a good electrical conductivity, a high specific surface area, a combination of charge storage mechanisms (associated with the electroadsorption and the Faradic reactions) and adequate control of the microstructuration can lead to synergetic effects which can drastically improve the electrochemical properties [25,26]. Different binary-composite films were assessed, employing various methods of preparation: high specific capacitances were attained with PANI-CNTs [27] or PEDOT-CNTs [28,29] composites; enhanced robustness of the flexible PPy-CNTs [30] or improved capacitive property of PTh-CNTs films [31] has also been revealed. Nevertheless, a deep understanding of the interfacial ionic transfer was not yet fully reached for these binary-composite materials. This is the reason why new methods of investigation are necessary to further improve their performances.

Taking into account the recent advances in the field of capacitive charge storage, on one hand, fabrication of composite electrodes with high specific surface area appears to be a key development path to achieve better SC performances. On the other hand, understanding the principles governing the ionic exchange mechanisms in nanostructured supercapacitor electrodes is equally important to shed light on this path and improve current devices. Therefore, suitable morphological, compositional as well as electrochemical characterization tools should be employed to assess composite electrode designs and the processes occurring at the electrode/electrolyte interface. For this purpose, various sophisticated analytical techniques have been developed to survey electrode–electrolyte interfaces that mainly govern the electrochemical operation of energy devices. Among them, the electrochemical quartz crystal microbalance (EQCM) [32–36] provides gravimetric changes of electrodes during electrochemical characterizations (such as charge/discharge) and offers

valuable insights of the interfaces, once the required conditions of the deposited film in terms of viscoelastic and hydrodynamic properties are included [37–39].

Therefore, this work focuses on the understanding of the processes occurring at the electrode/–electrolyte interfaces of composite electrode materials by using EQCM-based coupled electrochemical methods. Carbon- and CP-based composites (SWCNT/PPy) are prepared by the electrochemical synthesis of doped polypyrrole on the single-wall CNT-based networks, the latter providing a high specific surface area. Interfacial properties are characterized not only with gravimetric EQCM but also with its coupling with electrochemical impedance spectroscopy (EIS), the so-called *Ac*-electrogravimetry [40,41]. This complementary method can deliver unique species-selective and frequency-dependent information about the ionic exchange mechanisms at the electrode/electrolyte interface [42–44]. The processes occurring at SWCNT/PPy composite electrode/electrolyte interface, which are related to their pseudo-capacitive charge storage behavior, are discussed in comparison to their pristine components (i.e., SWCNT [32] and PPy [45,46]).

2. Materials and Methods

2.1. Materials

Single-wall CNT (755117-1G, length: 300–2300 nm and diameter: 0.7–1.1 nm), sodium dodecyl sulfate (NaDS), pyrrole monomer, sodium chloride and N-methylpyrrolidone (NMP) solvent were acquired from Sigma-Aldrich. Poly(vinylidene fluoride)-co- hexafluoropropylene (PVDF-HFP) is obtained from Solef® 21508, Solvay Solexis, Milan, Italy.

2.2. SWCNT/Polypyrrole Composite Thin Film Electrode Preparation

In the first step, the SWCNT film preparation was performed based on a method described in the literature [47,48]. SWCNTs were deposited by the "drop-casting" on a gold electrode (effective surface area of 0.2 cm^2) of a quartz crystal resonator (9 MHz, AW Sensors, Valencia, Spain), from a slurry containing 90% SWCNT powder and 10% PVDF-HFP (Poly(vinylidene fluoride-hexafluoropropylene)) polymer binder in N-methyl-2-pyrrolidone. A slurry containing 9 mg SWCNT powder, 1 mg of PVDF-HFP in 10 mL of NMP was ultrasonicated for about 20 min. Around 8 µL of this slurry was deposited on the gold electrode of the QCM. Then, the carbon films were subjected to a heat treatment at 120 °C for 30 min, with a heating rate of ~5 °C·min^{-1} to evaporate the residual solvent and improve the adhesion properties of the films on a gold electrode. The film thickness was estimated to be around 500 nm (based on field emission gun scanning electron microscopy (FEG-SEM) analyses, Figure 1). In a second step, the composite films of SWCNT/polypyrrole were obtained, following a method described in the literature [49]. The procedure consists of cycling the SWCNT electrode, previously prepared, in a solution containing 0.1 M pyrrole (freshly distilled) and 0.05 M sodium dodecyl sulfate (NaDS), at a scan rate of 0.01 V·s^{-1} in a potential range from 0 V to 0.675 V vs. Ag/AgCl during 2 cycles. The resulting films are taken out of the 3-electrode cell, rinsed with double distilled water and dried by purging with N_2 flow.

2.3. Morphological and Physical Characterizations

Prior to the thin film preparation, the SWCNT powders were characterized using nitrogen adsorption (the specific surface area was estimated at ~842 $m^2 \cdot g^{-1}$, by using Brunauer–Emmett–Teller (BET) analysis), X-ray diffraction (XRD) and high-resolution transmission electron microscopy (HRTEM). The morphological and structural observations, not shown here, were already given in Reference [34]. The surface morphology of the SWCNT/polypyrrole, after thin-film formation on the gold electrode of the resonators, was investigated by field emission gun scanning electron microscopy (FEG-SEM) (Zeiss, Supra 55, Oberkochen, Germany).

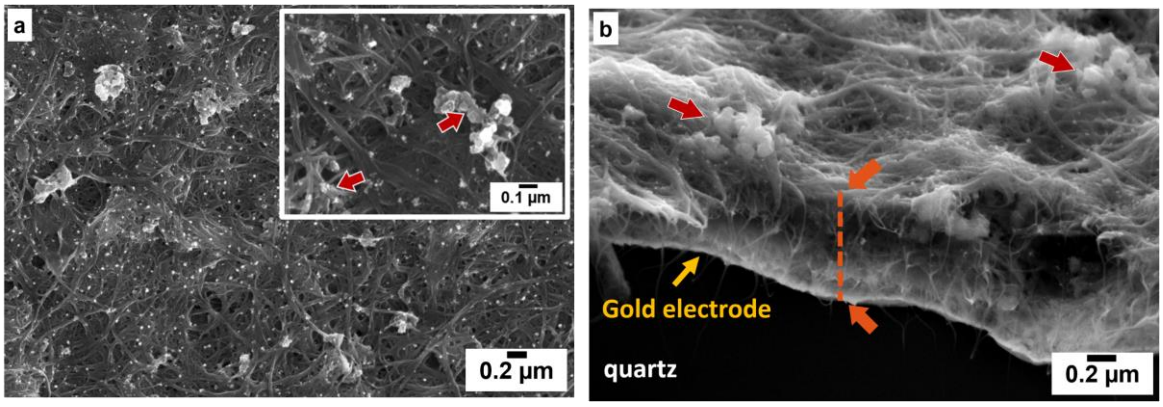

Figure 1. FEG-SEM images of single-wall carbon nanotubes/polypyrrole (SWCNT /PPy) nanocomposite film deposited on the gold electrode of a quartz resonator: (**a**) surface morphology with an inset showing the PPy clusters and (**b**) cross-section (red arrows point out the PPy clusters and orange colored arrows show the average film thickness).

2.4. Electrochemical and Electrogravimetric Characterizations

EQCM measurements were performed in 0.5 M NaCl (at pH = 7) in a three-electrode configuration. A lab-made QCM device was used to measure the microbalance frequency shift (Δf). Gold deposited on the quartz resonator was used as the working electrode. Platinum grid and Ag/AgCl (3 M KCl) was used as a counter and a reference electrode, respectively. The gravimetric conditions for the QCM analyses were assured by keeping film thickness acoustically thin (d_f < 500 nm) (Figure 1).

Ac-electrogravimetric measurements were also performed in the same three-electrode configuration described above. A four-channel frequency response analyzer (FRA, Solartron 1254) and a lab-made potentiostat (SOLETEM-PGSTAT) were used. The QCM was performed under a dynamic regime, and the modified working electrode was polarized at selected potentials to which a sinusoidal small-amplitude potential perturbation was superimposed. The frequency range was between 63 kHz and 10 mHz. The mass change, Δm, of the working electrode was measured simultaneously with the AC response, ΔI, of the electrochemical system, which led to the electrogravimetric (mass/potential) transfer function (TF), $\frac{\Delta m}{\Delta E}(\omega)$, and the electrochemical impedance, $\frac{\Delta E}{\Delta I}(\omega)$, to be obtained simultaneously at a given potential and frequency modulation, f (pulsation, $\omega = 2\pi f$). The operation principle and the details of the *Ac*-electrogravimetric measurement setup have been described in previous papers [40,41,50].

3. Results and Discussion

3.1. Morphological Aspects of the SWCNT/PPy Composites

The SWCNT/PPy composite electrodes are prepared in a two-step process. In a first step, a thin layer of SWCNT is formed on the gold electrode of the quartz resonators by drop-casting a slurry containing SWCNT and PVDF-HFP as an active material and as a binder, respectively. The morphological characteristics of the SWCNT-modified QCM resonators were previously discussed [34]. Briefly, N_2 adsorption analysis indicates that the SWCNTs have a pore diameter of 1–2 nm and a high specific surface area (~842 $m^2 \cdot g^{-1}$). Thin layers formed using these SWCNTs present a network of CNT bundles, made of at least ~10–20 CNTs [34]. In the second step, SWCNT-modified QCM resonators were used as a working electrode for the electropolymerization of pyrrole monomer, leading to the SWCNT/PPy composites. The surface morphology of SWCNT/polypyrrole (PPy) thin films was characterized by FEG-SEM, as shown in Figure 1. The images reveal a high-density of CNT bundles as it was already seen under the same film preparation conditions [34]. After two cycles (cyclic voltammetry) of PPy electrodeposition on the SWCNT-based electrodes, the formation of polypyrrole clusters with typical cauliflower or nodular morphology is observed in agreement with the previous studies [45], which

is more evident on certain locations on the film surface (Figure 1a inset and Figure 2b, indicated with red arrows).

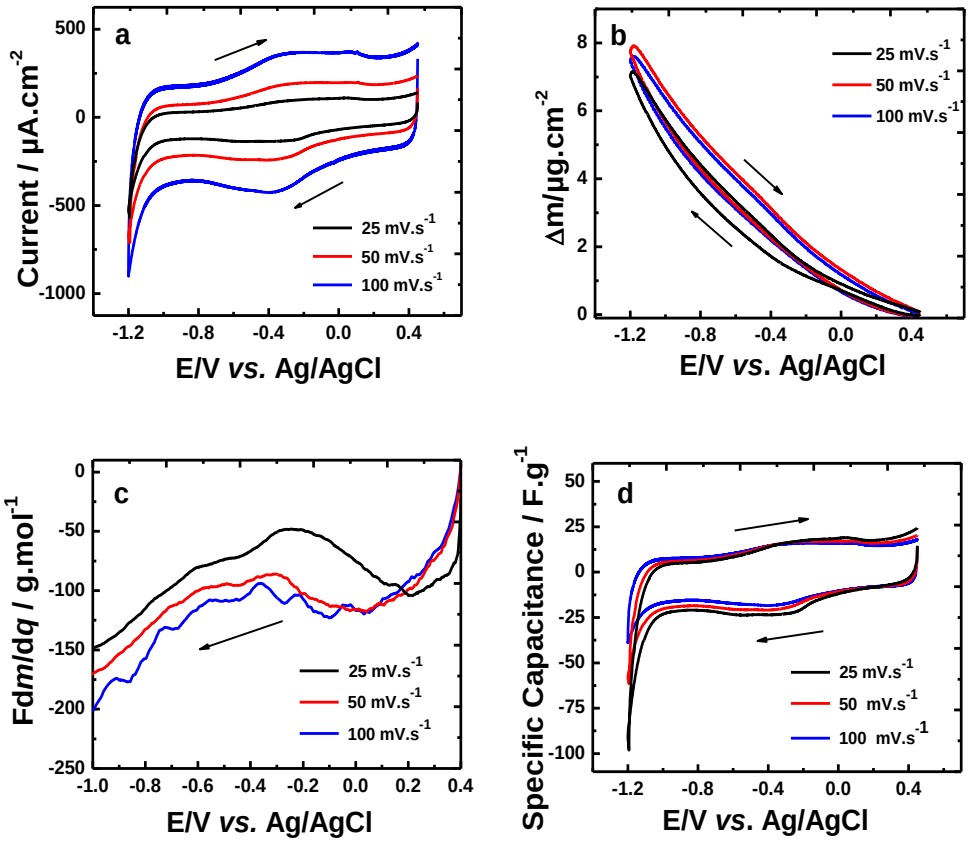

Figure 2. EQCM results of SWCNT/PPy composite thin films: (**a**) current vs. potential; (**b**) mass variation vs. potential; (**c**) calculated $F\frac{dm}{dq}$ values vs. potential; (**d**) specific capacitance values (calculated from panel **a**) vs. potential. Measurements in aqueous electrolyte 0.5 M NaCl pH 7.0 at 3 different scan rates.

The cross-section of the SWCNT/PPy shown in Figure 1b permits the composite thin-film thickness (d_f) to be estimated. The thickness is slightly inhomogeneous along the thin film and presents a variation from 450 to 550 nm. The electrodeposited PPy component (only two cycles of electrodeposition) on the SWCNTs does not significantly change the film thickness, and therefore, the gravimetric conditions are kept for the QCM based analysis. It is important to note that the composite film thickness is mainly governed by the SWCNT layer under these experimental conditions. Although the exact location of PPy electrodeposition is difficult to pronounce, it likely occurs on the porous surface of the network formed by the SWCNTs, rather than forming a second compact layer on top of the former.

3.2. EQCM Study of the SWCNT/PPy Composites

Classical EQCM studies were already performed for pristine SWCNT films in NaCl electrolytes, as shown in [32,34]. In these experiments, the appropriate potential range was selected from –0.4 V vs. Ag/AgCl to 0.4 V vs. Ag/AgCl. The current response reveals a classic square shape with bumps, while the mass change corresponds to a V-shape type: in the cathodic part, a cation/solvent contribution is observed, and on the contrary, an anion/solvent contribution was distinguished in the anodic region. A permselectivity failure, indicating a mixed contribution of cations and anions, is also seen around the point of zero charges (PZC)/point of zero mass (PZM), corresponding to a potential of +0.1 V vs. Ag/AgCl. The maximum mass variation is less than 1 µg·cm^{-2} in the case of the cation response and starting from this potential reference. In light of these results, an EQCM

analysis of the SWCNT/PPy composites was performed. The SWCNT/PPy composite film is oxidized and reduced between 0.45 V and −1.2 V vs. Ag/AgCl at three different scan rates of 25 mV·s^{-1}, 50 mV·s^{-1} and 100 mV·s^{-1} in 0.5 M NaCl solution (pH = 7). Figure 2a,b show the corresponding current and the mass changes, respectively. A slight contribution of the PPy component is apparently observed in the CV responses (Figure 2a), as compared to that of pristine SWCNTs [32]. Indeed, the current evolution is smoother or less bumpy in the case of the composite film, for example, when the region around −0.2 V vs. Ag/AgCl is examined. On the contrary, the mass response of the film is totally different in terms of amplitude and shape. Previous EQCM studies on pristine SWCNT in the same electrolyte have shown a V-shaped mass response around the PZC, which is around 0.1 V vs. Ag/AgCl [32]. Instead, here, for the composite film, the mass response shows only one slope; even a larger potential range has been examined. When the composite film was reduced, a larger mass increase was observed: a factor of four is observed between the amplitudes of composite and pristine SWCNTs for the same potential range. On the other hand, the anion contribution is completely removed here for the same potential range (Figure 2b), which was observed for the pristine SWCNT film from +0.2 to +0.4 V vs. Ag/AgCl. When the composite film is oxidized, the mass decreases all the time, while in the case of pristine SWCNTs, the mass increases for the higher potentials revealing an anion contribution, as already demonstrated [32]. These qualitative remarks already show that the presence of PPy changes the interfacial ion-exchange behavior of the SWCNTs.

Figure 2c shows the $F\frac{dm}{dq}\left(=F\frac{dm}{dt}\times\frac{1}{i}\right)$ function calculated from the EQCM data as a function of potential, which is equivalent to the global molar mass of the species obtained from the reduction branch in the range from 0.4 V to −1.2 V vs. Ag/AgCl in 0.5 M NaCl. At the cathodic potential region, the values vary in the range of 50–200 g·mol$^{-1,}$ which could correspond to Na^+ with a high number of hydration or Na^+ accompanied by free solvent molecules. However, at the anodic potentials, the values are smaller, and they vary in the range 0–50 g·mol^{-1}, which is also difficult to be attributed to a single ion contribution (i.e., 23 g·mol^{-1} and 35 g·mol^{-1}, for Na^+ and Cl^-, respectively). Unfortunately, using EQCM alone to understand the interfacial process appears to be limited in the present case because the charge compensation can also be due to the concomitant insertion of anions or to solvated cations or to a mixture of these species. Dynamic approaches have the potential to reach a fair separation of these processes (identification by the kinetic transfers). For this reason, *Ac*-electrogravimetric investigations were performed to complement the EQCM and will be discussed in Section 3.3.

Figure 2d depicts the variation of specific capacitance values as a function of the applied potential under the same conditions as mentioned previously. The gravimetric specific capacitance values (C_s) are estimated to be around 25 to 30 F·g^{-1} in the range from −1.0 V to +0.45 V vs. Ag/AgCl. For very cathodic potentials, reduction of water interferes in the CV curves and thus, strongly modify the C_s values. Otherwise, these C_s are in the same order of magnitude as that obtained with pristine SWCNT thin-film electrodes [34,51,52].

A small dependence on the scan rate values is observed in the EQCM responses, which is more pronounced in the $F\frac{dm}{dq}$ the function is shown in Figure 2c. This result suggests that depending on the scan rate, different species may contribute to the electroadsorption and/or faradaic processes. Indeed, the information provided by the classical EQCM is insufficient for a thorough explanation of the transfer mechanism of the different species. As *Ac*-electrogravimetry was proven to be a strong complementary tool to EQCM in the previous CNT studies [32–34], the composite films were also analyzed with this technique. As mentioned earlier, this coupled tool can deliver unique species-selective and frequency-dependent information about the ion exchange mechanisms at the electrode/electrolyte interface.

3.3. Ac-Electrogravimetric Study of the SWCNT/PPy Composites

With the *Ac*-electrogravimetric approach, an EQCM response deconvolution was performed with the pristine SWCNT, as shown in references [32,34]. Briefly, the contribution of $Na^+.H_2O$, H^+ and Cl^- were detected when the surface is negatively and positively charged, respectively. The faster interfacial transfer is obtained for the $Na^+.H_2O$ and Cl^- species. H_2O was observed at lower kinetics of transfer, whereas H^+ was seen at very low values. In terms of quantities, major contributions are due to hydrated sodium with a quasi-equivalent contribution of water in the cathodic part and a lesser proton and chloride contributions. These findings are compared below to those obtained with the SWCNT/PPy composite electrodes.

The measurements were performed at each 200 mV in the range from 0.4 V to −1.2 V vs. Ag/AgCl in 0.5 M NaCl electrolyte. Figure 3 shows an example of the experimental and theoretical electrochemical transfer functions (TFs) obtained from *Ac*-electrogravimetry of an SWCNT/PPy thin film in 0.5 M NaCl electrolyte at −0.4 V vs. Ag/AgCl. The experimental data were fitted according to the model presented briefly in Appendix A (theoretical part). More details about the theory can be found in previous works [40,41]. A Mathcad software® was used to perform this step, assuring a good fitting for all the transfer functions measured at a given potential and by using the same set of parameters.

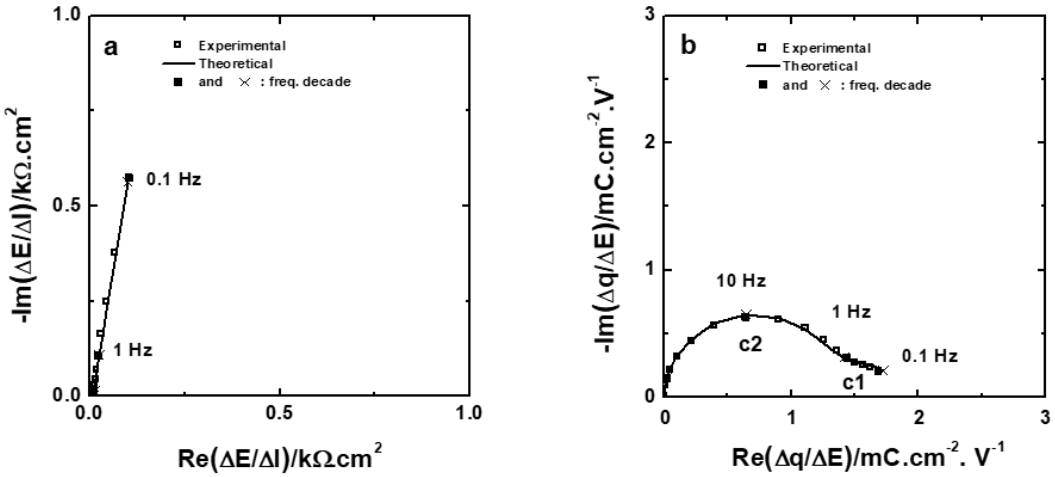

Figure 3. Experimental and theoretical electrochemical data of the SWNT/PPy thin film in 0.5 M NaCl measured at −0.4 V vs. Ag/AgCl: (**a**) electrochemical impedance, $\frac{\Delta E}{\Delta I}(\omega)$ and (**b**) charge/potential transfer function, $\frac{\Delta q}{\Delta E}(\omega)$. Theoretical functions were calculated with the following parameters: $d_f = 0.4$ µm, $K_{c1} = 9.50 \times 10^{-5}$ cm·s^{-1}, $G_{c1} = 7.98 \times 10^{-9}$ mol·s^{-1}·cm^{-2}·V^{-1}, $K_{c2} = 3.46 \times 10^{-3}$ cm·s^{-1} and $G_{c2} = 9.3 \times 10^{-7}$ mol·s^{-1}·cm^{-2}·V^{-1}.

A good agreement between experimental data and theoretical curves are evident in Figure 3. The electrochemical impedance, $\frac{\Delta E}{\Delta I}(\omega)$ (Figure 3a), present a slightly distorted straight line at the lower frequency domain, indicating that there is a multi-ion transfer contribution. Therefore, it is difficult to extract information from this transfer function. The charge/potential transfer function, $\frac{\Delta q}{\Delta E}(\omega)$ (Figure 3b), permit an easier separation of the ionic contributions, however, without any possibility to identify the ionic species involved. Figure 3b shows two loops, which can be attributed to at least two species, where their time constants are not sufficiently different from each other to obtain perfectly separated loops. Here, a big loop is observed around a characteristic frequency of 10 Hz, followed by a smaller one appearing at low frequencies. Equations (A1) and (A2) given in Appendix A were used here for the fitting process, assuming the contribution of two ions named c1 and c2. At this level, these two transfer functions, $\frac{\Delta E}{\Delta I}(\omega)$ and $\frac{\Delta q}{\Delta E}(\omega)$, are similar to those obtained with pristine SWCNTs under the same experimental conditions of measurements [32].

In the mass/potential transfer function, $\frac{\Delta m}{\Delta E}(\omega)$, one big loop appears in the third quadrant (Figure 4), which is characteristic for cation/solvated cation contributions or free solvent molecules in the same flux direction. In the fitting process of the experimental $\frac{\Delta m}{\Delta E}(\omega)$, three species are considered: $Na^+.nH_2O$ at higher frequencies, free H_2O molecules at intermediate frequencies and H^+ at lower frequencies. The identification of these species was achieved by the determination of their molar mass, M_i, using Equation (A3) given in the theoretical part of Appendix A. The two parameters K_i and G_i, were already given by the electrochemical response for the two ionic species. For the free solvent, K_s and G_s are only estimated through the mass/potential transfer function, $\frac{\Delta m}{\Delta E}(\omega)$.

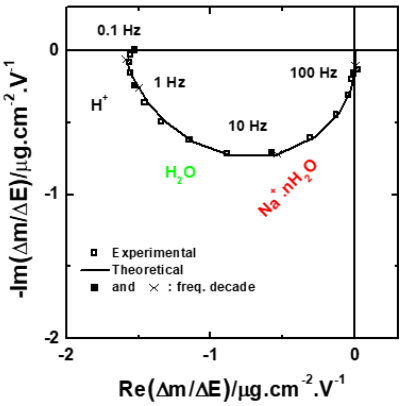

Figure 4. Experimental and theoretical electrogravimetric transfer function, $\frac{\Delta m}{\Delta E}(\omega)$, of the SWNT/PPy thin film in 0.5 M NaCl measured at −0.4 V vs. Ag/AgCl. Theoretical function was calculated with the following parameters: d_f = 0.4 μm, $K_{c1} = 9.50 \times 10^{-5}$ cm·s^{-1}, $G_{c1} = 7.98 \times 10^{-9}$ mol·s^{-1}·cm^{-2}·V^{-1}, $K_{c2} = 3.46 \times 10^{-3}$ cm·s^{-1}, $G_{c2} = 9.3 \times 10^{-7}$ mol·s^{-1}·cm^{-2}·V^{-1}, $K_s = 1.97 \times 10^{-3}$ cm·s^{-1}, $G_s = 1.99 \times 10^{-6}$ mol·s^{-1}, M_{c1} = 1 g·mol^{-1}, M_{c2} = 23 + 18 g·mol^{-1} and M_s = 18 g·mol^{-1}.

The contribution of three different species in the charge compensation process, estimated by fitting the experimental data, was further confirmed by carefully analyzing the partial electrogravimetric transfer function. For example, the cation 1, c1, the contribution is removed and $\left.\frac{\Delta m}{\Delta E}\right|^{c2s}(\omega)$ is calculated or the cation 2, c2, the contribution is removed and $\left.\frac{\Delta m}{\Delta E}\right|^{c1s}(\omega)$ is calculated (Equations (A3) and (A4)). Figure 5a,b exhibit a good agreement between the theoretical and experimental data. These partial electrogravimetric transfer functions provide a crosscheck for validating the hypothesis involving three different species and a better separation of the various contributions. If the molar masses chosen to identify the species are different from reality, a good agreement cannot be obtained. It should be noted that for $\left.\frac{\Delta m}{\Delta E}\right|^{c1s}(\omega)$, a small loop appears in the fourth quadrant at low frequencies. According to our calculation, this response is related to the proton contribution, and normally, the cation response is located at the third quadrant of the Cartesian coordinates system. This difference is due to the mathematic treatment observed in Equation (A4) where a factor of M_{c1}-M_{c2} appears; in our case, a negative value is obtained as the molar mass of c2 (hydrated sodium) is higher than the molar mass of c1 (proton). Thus, the response is located at this part of the complex plane, which appears as a virtual anion contribution. Since we have a perfect agreement for all the TFs, our model used in the fitting process is confirmed to be valid at this potential (−0.4 V vs. Ag/AgCl). This procedure was followed for different potentials in the potential range used for the EQCM measurements. The key parameters, K_i, G_i and M_i, are obtained for all the species involved directly or indirectly in the charge compensation process.

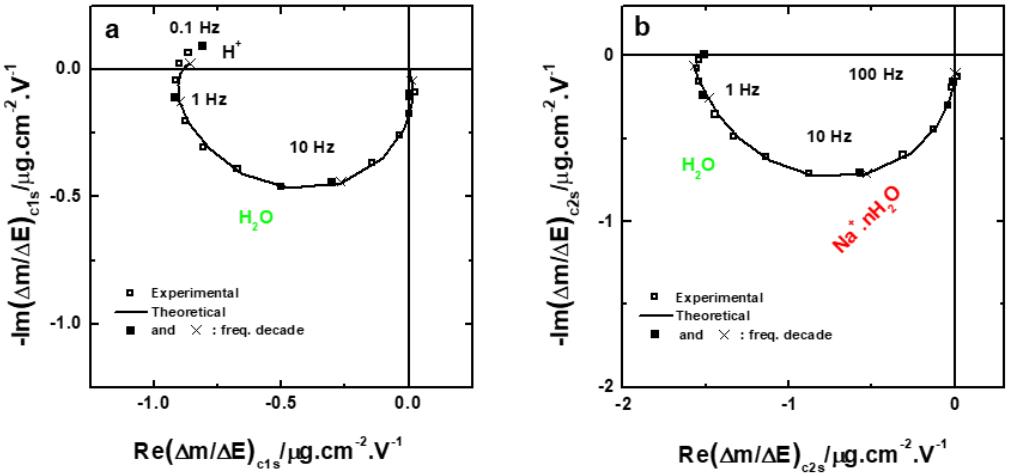

Figure 5. Partial electrogravimetric transfer function of the SWNT-PPy thin film in 0.5 M NaCl measured at −0.4 V vs. Ag/AgCl: (**a**) $\left.\frac{\Delta m}{\Delta E}\right|^{c1s}(\omega)$ cation1-solvent partial transfer function and (**b**) $\left.\frac{\Delta m}{\Delta E}\right|^{c2s}(\omega)$ cation2-solvent partial transfer function. Theoretical functions were calculated with the same set of parameters used previously for the data presented in Figures 3 and 4.

For potentials more cathodic than −0.3 V vs. Ag/AgCl, the contribution of only three species is found mixing the two cations, $Na^+.nH_2O$ and H^+, and free solvent molecules following the same transfer direction. On the contrary, for more anodic potential values, the proton contribution vanishes, and chloride species appear at very low frequencies.

Figure 6a,b display how the kinetic transfer rates, K_i, and the transfer resistance, Rt_i, of the species evolve as a function of the applied potential. The potential range corresponds to the conditions where the electroadsorption/desorption or insertion/expulsion processes of the thin film can be observed. The K_i values presented in Figure 6a indicate that the $Na^+.nH_2O$ ion is the fastest of the four species. This observation may be correlated to an easier dehydration process of the sodium species compared to the protons. For the latter ions, it is noted that their corresponding interfacial transfer occurs at low frequencies. Additionally, the concentration of the protons in the electrolyte is much lower compared to that of sodium species at this pH value.

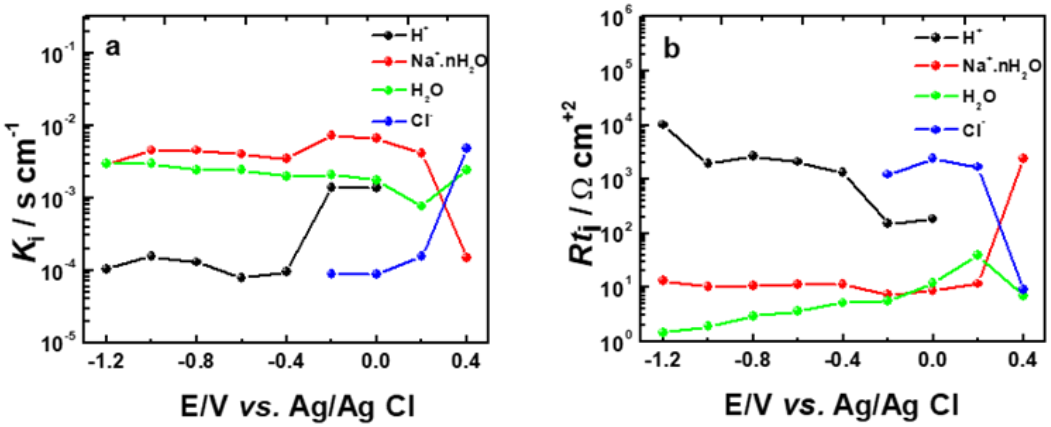

Figure 6. The kinetic transfer constants, K_i, and transfer resistance, Rt_i, for all species estimated from the fitting of the *Ac*-electrogravimetric data of SWCNT/PPy composite measured in 0.5 M NaCl: (**a**) kinetic transfer constants, K_i and (**b**) transfer resistance, Rt_i.

Furthermore, the kinetic transfer rates, K_s, of free water molecules are somewhat close to the values of the $Na^+.nH_2O$ ions. As for the Cl^- ions, their transfer occurs at low frequencies and only at more anodic potentials.

In SWCNT/PPy composites, the kinetic transfer rates, K_i, of $Na^+.nH_2O$ are significantly lower than the K_i of the $Na^+.nH_2O$ in pristine SWCNTs [32] and higher than the K_i of the Na^+ species detected in pristine PPy [45,49], measured under similar conditions. These results indicate that the composite structure does not hinder the sodium species transfer, and probably it is governed by the insertion process in PPy rather than a faster electroadsorption/desorption process. Additionally, the contribution of the sodium species to the charge compensation process (both electrostatic and faradaic) is enlarged to the whole potential range, i.e., 0.4 V to −1.2 V vs. Ag/AgCl (larger than that used for SWCNTs alone), but at the expense of their kinetics.

For the other species, the following trends were observed: (i) the kinetic transfer rates, K_c, of the H^+ in the SWCNT/PPy are faster than the kinetic transfer rates of H^+ in the SWCNT and (ii) the kinetic transfer rates, K_a, of the Cl^- in the SWCNT/PPy are more or less equivalent to the kinetic transfer rates of the Cl^- in the SWCNT [32] and in the pristine doped PPy [46].

In view of the transfer resistance values, Rt_i, of the ions, the $Na^+.nH_2O$ species from the SWCNT/PPy are slightly more difficult to be transferred compared with the $Na^+.nH_2O$ species in the SWCNT: 10 ohms·cm^2 in Figure 6b versus 2 ohms·cm^2, previously given in [32]. The Rt_i of H^+ in the SWCNT/PPy composite is more or less equivalent to that in pristine SWCNT. The Rt_i of Cl^- in the SWCNT/PPy composite is comparable to that obtained in pristine SWCNT [32] and that found in doped PPy electrodes [46].

Taking into consideration of the K_i and Rt_i values of various species detected, one can suggest that there is no major hindrance of the ions transfer when doped PPy is deposited on the SWCNT electrodes. The species detected are related to the electroactivity of the two components. For example, at the anodic potentials, there is no cation contribution in pristine SWCNTs, whereas it exits in the composite structure due to the PPy.

Figure 7 displays the relative concentration change for the ionic species detected in the *Ac*-electrogravimetric measurements. The C_i-C_0 values for H_2O are significantly higher than the C_i-C_0 values of $Na^+.nH_2O$, H^+ and Cl^-. The relative concentration change of the $Na^+.nH_2O$ in SWCNT/PPy is equivalent to the C_i-C_0 values of the $Na^+.nH_2O$ in pristine SWCNT. These values agree well with the C_i-C_0 values of Na^+ detected in doped PPy structures [46]. The same trend was observed for H^+ and Cl^- anions, C_i-C_0 values of the H^+ and Cl^- did not significantly vary in the SWCNT/PPy composite compared to pristine SWCNTs [32]. The C_i-C_0 values of the free solvent in the SWCNT–PPy composite are significantly higher than the C_i-C_0 values of the free solvent in the SWCNT. These values are rather similar to that obtained for doped PPy thin films studied in our group [46], which indicates that the water transfer is principally governed by the doped PPy of the composite electrode.

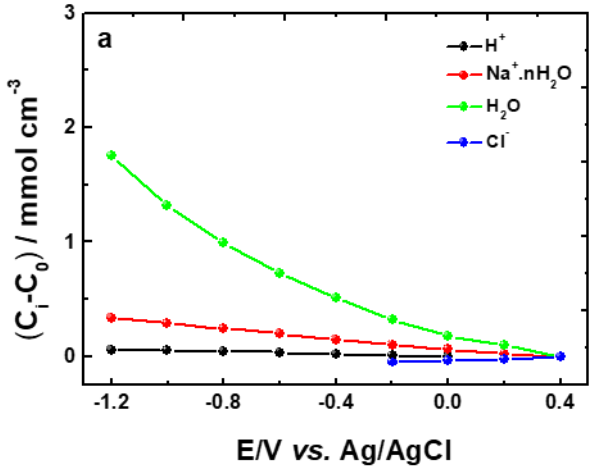

Figure 7. Evolution of the relative concentration, C_i-C_0 of each species over the potential applied measured in 0.5 M NaCl SWCNT/PPy.

Solely evaluating the electrochemical signatures of the pristine SWCNT and SWCNT/PPy composites does not allow us to distinguish the improvements in terms of interfacial species transfer behavior. Therefore, the main novelty of the present study is the way of characterization of the electrode/electrolyte interface by combining EQCM with simultaneous EIS measurements, providing a gravimetric and dynamic deconvolution of the interfacial processes. The results of the advanced electrogravimetric study revealed the differences between the pristine and composite electrodes relative to their charge compensation mechanism. The clarified points include the enlargement of the usable potential window and the enhanced permselectivity of the SWCNT/PPy composites compared to those of pristine SWCNTs, which could be revealed thanks to the advanced electrogravimetric tools (EQCM and its EIS coupling) used in our study.

4. Conclusions

Globally, the signature of PPy in the SWCNT/PPy composite is not very visible, both in current and mass response. Only after a closer examination, it can be seen that this composite SWCNT/PPy film has a much-improved response compared to pristine SWCNT and PPy films tested under the same conditions. These subtleties can be summarized as follows:

- The range of usable potential is greater for composite SWCNT/PPy films than for SWCNT films, particularly for the cathodic part, since it is possible to push this limit further (more cathodic potentials than -0.6 V vs. Ag/AgCl) before reaching solvent degradation under the same experimental conditions. This should allow a higher storage capacity to be obtained. This effect is also confirmed by mass variation measurements via the responses given by the quartz microbalance tool;
- The mass change obtained with composite SWCNT/PPy films is much higher than that observed for pristine SWCNT films if this mass variation is considered as a whole. However, this observation should be moderated because the most cathodic potential that can be achieved with these composite films is much lower compared to the tests on SWNCT films. Nevertheless, if the same potential range is examined, classically from -0.4 V vs. Ag/AgCl to +0.4 V vs. Ag/AgCl, the amount of (co)electroadsorbed species is still four times greater;
- The permselectivity is also greatly improved in the case of composite SWCNT/PPy films compared to SWCNT films. This is, on one hand, confirmed by the shape of the Δm-E response, given by the EQCM measurements, which is monotonically decreasing for composite SWCNT/PPy films while it has a classical "V" shape around the PZC for SWCNT films. The part corresponding to the most anodic potentials is mainly related to the electroadsorbed anions. In the case of the composite SWCNT/PPy films, this contribution is clearly very small. On the other hand, the quantities of anions estimated by *Ac*-electrogravimetric measurements are much lower in the case of composites. This corroborates the better permselectivity of these composite SWCNT/PPy films even with a moderate amount of PPy.

Author Contributions: F.E.-T. performed the experiments; H.P. and O.S. planned the experiments; F.E.-T., H.P and O.S analyzed the data; H.P. and O.S. contributed to the original draft preparation and revision; O.S. wrote, revised and edited the paper with discussions mainly with H.P. All authors have read and agreed to the published version of the manuscript.

Funding: F.E.-T. thanks the (Secrétariat National pour l'Enseignement Supérieur, la Science, la Technologie et l'Innovation (SENESCYT)-Equateur for the financial support during his Ph.D. thesis.

Acknowledgments: The authors thank Francoise Pillier for the FEG-SEM measurements.

Conflicts of Interest: The authors declare no conflict of interest.

Appendix A

The experimental data of the electrochemical impedance, $\frac{\Delta E}{\Delta I}(\omega)$, and the charge/potential TF, $\frac{\Delta q}{\Delta E}(\omega)$, were fitted using theoretical functions given in Equations (A1) and (A2). It is considered here that only two ions, $c1$ and $c2$, are involved in the charge compensation process.

$$\left.\frac{\Delta E}{\Delta I}\right|_{\text{th}}(\omega) = \left[j\omega d_{\text{f}}\left(\frac{G_{\text{c1}}}{j\omega d_{\text{f}}+K_{\text{c1}}}+\frac{G_{\text{c2}}}{j\omega d_{\text{f}}+K_{\text{c2}}}\right)\right]^{-1} \tag{A1}$$

$$\left.\frac{\Delta q}{\Delta E}\right|_{\text{th}}(\omega) = d_{\text{f}}F\left(\frac{G_{\text{c1}}}{j\omega d_{\text{f}}+K_{\text{c1}}}+\frac{G_{\text{c2}}}{j\omega d_{\text{f}}+K_{\text{c2}}}\right) \tag{A2}$$

where d_{f} is the film thickness, K_{i} represents the kinetics rate of transfer, whereas G_{i} describes the level of difficulty corresponding to this transfer for each ionic species, $c1$ and $c2$ in our case, transferred at the electrode/electrolyte interface. For the parameter G_{i}, an analogy with a transfer resistance is generally used: $Rt_{\text{i}} = \frac{1}{FG_{\text{i}}}$.

The theoretical electrogravimetric transfer function, $\frac{\Delta m}{\Delta E}(\omega)$, can be calculated, taking into account the charged/uncharged species contribution:

$$\left.\frac{\Delta m}{\Delta E}\right|_{\text{th}}(\omega) = d_{\text{f}}\left(M_{\text{c1}}\frac{G_{\text{c1}}}{j\omega d_{\text{f}}+K_{\text{c1}}}+M_{\text{c2}}\frac{G_{\text{c2}}}{j\omega d_{\text{f}}+K_{\text{c2}}}+M_{\text{s}}\frac{G_{\text{s}}}{j\omega d_{\text{f}}+K_{\text{s}}}\right) \tag{A3}$$

In Equation (A3), additional parameters, K_{s} and G_{s} for the solvent molecules are added as the molar mass (M_{i}) of each species.

From the theoretical overall electrogravimetric transfer function (Equation (A3)), it is possible to calculate the theoretical partial transfer functions by removing the $c2$ contribution, calculating $\left.\frac{\Delta m}{\Delta E}\right|_{\text{th}}^{\text{c1s}}(\omega)$; or the $c1$ contribution, calculating $\left.\frac{\Delta m}{\Delta E}\right|_{\text{th}}^{\text{c2s}}(\omega)$, as shown in the following equations:

$$\left.\frac{\Delta m}{\Delta E}\right|_{\text{th}}^{\text{c1s}}(\omega) = d_{\text{f}}\left((M_{\text{c1}}-M_{\text{c2}})\frac{G_{\text{c1}}}{j\omega d_{\text{f}}+K_{\text{c1}}}+M_{\text{s}}\frac{G_{\text{s}}}{j\omega d_{\text{f}}+K_{\text{s}}}\right) \tag{A4}$$

$$\left.\frac{\Delta m}{\Delta E}\right|_{\text{th}}^{\text{c2s}}(\omega) = d_{\text{f}}\left((M_{\text{c2}}-M_{\text{c1}})\frac{G_{\text{c2}}}{j\omega d_{\text{f}}+K_{\text{c2}}}+M_{\text{s}}\frac{G_{\text{s}}}{j\omega d_{\text{f}}+K_{\text{s}}}\right) \tag{A5}$$

References

1. Xue, Y.; Chen, S.; Yu, J.R.; Bunes, B.R.; Xue, Z.X.; Xu, J.K.; Lu, B.Y.; Zang, L. Nanostructured conducting polymers and their composites: Synthesis methodologies, morphologies and applications. *J. Mater. Chem. C* **2020**, *8*, 10136–10159. [CrossRef]
2. Nair, S.S.; Mishra, S.K.; Kumar, D. Review—Polymeric materials for energy harvesting and storage applications. *Polymer-Plastics Technol. Mater.* **2020**. [CrossRef]
3. Simon, P.; Gogotsi, Y. Materials for electrochemical capacitors. *Nat. Mater.* **2008**, *7*, 845–854. [CrossRef] [PubMed]
4. Miller, J.R.; Simon, P. Electrochemical Capacitors for Energy Management. *Science* **2008**, *321*, 651–652. [CrossRef] [PubMed]
5. Wang, G.; Zhang, L.; Zhang, J. A review of electrode materials for electrochemical supercapacitors. *Chem. Soc. Rev.* **2012**, *41*, 797–828. [CrossRef] [PubMed]
6. Miller, J.R.; Burke, A. Electrochemical Capacitors: Challenges and Opportunities for Real-World Applications. *Electrochem. Soc. Interface* **2008**, *17*, 53–57. [CrossRef]
7. Zhang, L.L.; Zhao, X.S. Carbon-based materials as supercapacitor electrodes. *Chem. Soc. Rev.* **2009**, *38*, 2520–2531. [CrossRef]
8. Béguin, F.; Presser, V.; Balducci, A.; Frackowiak, E. Carbons and Electrolytes for Advanced Supercapacitors. *Adv. Mater.* **2014**, *26*, 2219–2251. [CrossRef]
9. Shao, H.; Wu, Y.-C.; Lin, Z.; Taberna, P.-L.; Simon, P. Nanoporous carbon for electrochemical capacitive energy storage. *Chem. Soc. Rev.* **2020**, *49*, 3005–3039. [CrossRef]
10. Han, L.; Tang, P.; Zhang, L. Hierarchical Co3O4@PPy@MnO2 core–shell–shell nanowire arrays for enhanced electrochemical energy storage. *Nano Energy* **2014**, *7*, 42–51. [CrossRef]
11. Xia, X.; Chao, D.; Fan, Z.; Guan, C.; Cao, X.; Zhang, H.; Fan, H.J. A New Type of Porous Graphite Foams and Their Integrated Composites with Oxide/Polymer Core/Shell Nanowires for Supercapacitors: Structural Design, Fabrication, and Full Supercapacitor Demonstrations. *Nano Lett.* **2014**, *14*, 1651–1658. [CrossRef] [PubMed]

12. Simon, P.; Gogotsi, Y. Capacitive Energy Storage in Nanostructured Carbon–Electrolyte Systems. *Acc. Chem. Res.* **2013**, *46*, 1094–1103. [CrossRef] [PubMed]
13. Davies, A.; Yu, A. Material advancements in supercapacitors: From activated carbon to carbon nanotube and graphene. *Can. J. Chem. Eng.* **2011**, *89*, 1342–1357. [CrossRef]
14. An, K.H.; Kim, W.S.; Park, Y.S.; Choi, Y.C.; Lee, S.M.; Chung, D.C.; Bae, D.J.; Lim, S.C.; Lee, Y.H. Supercapacitors Using Single-Walled Carbon Nanotube Electrodes. *Adv. Mater.* **2001**, *13*, 497–500. [CrossRef]
15. Li, P.; Yang, Y.; Shi, E.; Shen, Q.; Shang, Y.; Wu, S.; Wei, J.; Wang, K.; Zhu, H.; Yuan, Q.; et al. Core-Double-Shell, Carbon Nanotube@Polypyrrole@MnO2 Sponge as Freestanding, Compressible Supercapacitor Electrode. *ACS Appl. Mater. Interfaces* **2014**, *6*, 5228–5234. [CrossRef]
16. Zeng, S.; Chen, H.; Cai, F.; Kang, Y.; Chen, M.; Li, Q. Electrochemical fabrication of carbon nanotube/polyaniline hydrogel film for all-solid-state flexible supercapacitor with high areal capacitance. *J. Mater. Chem. A* **2015**, *3*, 23864–23870. [CrossRef]
17. Mo, D.; Zhou, W.; Ma, X.; Xu, J.; Zhu, D.; Lu, B. Electrochemical synthesis and capacitance properties of a novel poly(3,4-ethylenedioxythiophene bis-substituted bithiophene) electrode material. *Electrochim. Acta* **2014**, *132*, 67–74. [CrossRef]
18. Feng, H.; Wang, B.; Tan, L.; Chen, N.; Wang, N.; Chen, B. Polypyrrole/hexadecylpyridinium chloride-modified graphite oxide composites: Fabrication, characterization, and application in supercapacitors. *J. Power Sources* **2014**, *246*, 621–628. [CrossRef]
19. Liu, T.; Finn, L.; Yu, M.; Wang, H.; Zhai, T.; Lu, X.; Tong, Y.; Li, Y. Polyaniline and Polypyrrole Pseudocapacitor Electrodes with Excellent Cycling Stability. *Nano Lett.* **2014**, *14*, 2522–2527. [CrossRef]
20. Ambade, R.B.; Ambade, S.B.; Shrestha, N.K.; Nah, Y.-C.; Han, S.-H.; Lee, W.; Lee, S.-H. Polythiophene infiltrated TiO_2 nanotubes as high-performance supercapacitor electrodes. *Chem. Commun.* **2013**, *49*, 2308–2310. [CrossRef]
21. Shen, J.; Li, T.; Huang, W.; Long, Y.; Li, N.; Ye, M. One-pot polyelectrolyte assisted hydrothermal synthesis of RuO_2-reduced graphene oxide nanocomposite. *Electrochim. Acta* **2013**, *95*, 155–161. [CrossRef]
22. Long, X.; Zeng, Z.; Guo, E.; Shi, X.; Zhou, H.; Wang, X. Facile fabrication of all-solid-state flexible interdigitated MnO_2 supercapacitor via in-situ catalytic solution route. *J. Power Sources* **2016**, *325*, 264–272. [CrossRef]
23. Bae, J.; Song, M.K.; Park, Y.J.; Kim, J.M.; Liu, M.; Wang, Z.L. Fiber supercapacitors made of nanowire-fiber hybrid structures for wearable/flexible energy storage. *Angew. Chem. Int. Ed. Engl.* **2011**, *50*, 1683–1687. [CrossRef]
24. Wang, D.-W.; Li, F.; Cheng, H.-M. Hierarchical porous nickel oxide and carbon as electrode materials for asymmetric supercapacitor. *J. Power Sources* **2008**, *185*, 1563–1568. [CrossRef]
25. Meng, Q.; Cai, K.; Chen, Y.; Chen, L. Research progress on conducting polymer based supercapacitor electrode materials. *Nano Energy* **2017**, *36*, 268–285. [CrossRef]
26. Shown, I.; Ganguly, A.; Chen, L.-C.; Chen, K.-H. Conducting polymer-based flexible supercapacitor. *Energy Sci. Eng.* **2015**, *3*, 2–26. [CrossRef]
27. Imani, A.; Farzi, G. Facile route for multi-walled carbon nanotube coating with polyaniline: Tubular morphology nanocomposites for supercapacitor applications. *J. Mater. Sci. Mater. Electron.* **2015**, *26*, 7438–7444. [CrossRef]
28. Zhou, Y.; Xu, H.; Lachman, N.; Ghaffari, M.; Wu, S.; Liu, Y.; Ugur, A.; Gleason, K.K.; Wardle, B.L.; Zhang, Q.M. Advanced asymmetric supercapacitor based on conducting polymer and aligned carbon nanotubes with controlled nanomorphology. *Nano Energy* **2014**, *9*, 176–185. [CrossRef]
29. Tahir, M.; He, L.; Haider, W.A.; Yang, W.; Hong, X.; Guo, Y.; Pan, X.; Tang, H.; Li, Y.; Mai, L. Co-Electrodeposited porous PEDOT–CNT microelectrodes for integrated micro-supercapacitors with high energy density, high rate capability, and long cycling life. *Nanoscale* **2019**, *11*, 7761–7770. [CrossRef] [PubMed]
30. Chen, Y.; Du, L.; Yang, P.; Sun, P.; Yu, X.; Mai, W. Significantly enhanced robustness and electrochemical performance of flexible carbon nanotube-based supercapacitors by electrodepositing polypyrrole. *J. Power Sources* **2015**, *287*, 68–74. [CrossRef]
31. Fu, C.; Zhou, H.; Liu, R.; Huang, Z.; Chen, J.; Kuang, Y. Supercapacitor based on electropolymerized polythiophene and multi-walled carbon nanotubes composites. *Mater. Chem. Phys.* **2012**, *132*, 596–600. [CrossRef]
32. Escobar-Teran, F.; Arnau, A.; Garcia, J.V.; Jiménez, Y.; Perrot, H.; Sel, O. Gravimetric and dynamic deconvolution of global EQCM response of carbon nanotube based electrodes by Ac-electrogravimetry. *Electrochem. Commun.* **2016**, *70*, 73–77. [CrossRef]
33. Escobar-Teran, F.; Perrot, H.; Sel, O. Charge storage properties of single wall carbon nanotubes/Prussian blue nanocube composites studied by multi-scale coupled electrogravimetric methods. *Electrochim. Acta* **2018**, *271*, 297–304. [CrossRef]
34. Escobar-Teran, F.; Perrot, H.; Sel, O. Ion Dynamics at the Single Wall Carbon Nanotube Based Composite Electrode/Electrolyte Interface: Influence of the Cation Size and Electrolyte pH. *J. Phys. Chem. C* **2019**, *123*, 4262–4273. [CrossRef]
35. Hillman, A.R. The EQCM: Electrogravimetry with a light touch. *J. Solid State Electrochem.* **2011**, *15*, 1647–1660. [CrossRef]
36. Tsai, W.-Y.; Taberna, P.-L.; Simon, P. Electrochemical Quartz Crystal Microbalance (EQCM) Study of Ion Dynamics in Nanoporous Carbons. *J. Am. Chem. Soc.* **2014**, *136*, 8722–8728. [CrossRef]
37. Shpigel, N.; Levi, M.D.; Sigalov, S.; Daikhin, L.; Aurbach, D. In Situ Real-Time Mechanical and Morphological Characterization of Electrodes for Electrochemical Energy Storage and Conversion by Electrochemical Quartz Crystal Microbalance with Dissipation Monitoring. *Acc. Chem. Res.* **2018**, *51*, 69–79. [CrossRef]
38. Shpigel, N.; Levi, M.D.; Aurbach, D. EQCM-D technique for complex mechanical characterization of energy storage electrodes: Background and practical guide. *Energy Storage Mater.* **2019**, *21*, 399–413. [CrossRef]
39. Levi, M.D.; Shpigel, N.; Sigalov, S.; Dargel, V.; Daikhin, L.; Aurbach, D. In Situ Porous Structure Characterization of Electrodes for Energy Storage and Conversion by EQCM-D: A Review. *Electrochim. Acta* **2017**, *232*, 271–284. [CrossRef]

40. Gabrielli, C.; Garcia-Jareno, J.J.; Keddam, M.; Perrot, H.; Vicente, F. Ac-electrogravimetry study of electroactive thin films. II. Application to polypyrrole. *J. Phys. Chem. B* **2002**, *106*, 3192–3201. [CrossRef]
41. Gabrielli, C.; García-Jareño, J.J.; Keddam, M.; Perrot, H.; Vicente, F. Ac-Electrogravimetry Study of Electroactive Thin Films. I. Application to Prussian Blue. *J. Phys. Chem. B* **2002**, *106*, 3182–3191. [CrossRef]
42. Arias, C.R.; Debiemme-Chouvy, C.; Gabrielli, C.; Laberty-Robert, C.; Pailleret, A.; Perrot, H.; Sel, O. New Insights into Pseudocapacitive Charge-Storage Mechanisms in Li-Birnessite Type MnO2 Monitored by Fast Quartz Crystal Microbalance Methods. *J. Phys. Chem. C* **2014**, *118*, 26551–26559. [CrossRef]
43. Lemaire, P.; Dargon, T.; Alves Dalla Corte, D.; Sel, O.; Perrot, H.; Tarascon, J.-M. Making Advanced Electrogravimetry as an Affordable Analytical Tool for Battery Interface Characterization. *Anal. Chem.* **2020**, *92*, 13803–13812. [CrossRef]
44. Lemaire, P.; Sel, O.; Alves Dalla Corte, D.; Iadecola, A.; Perrot, H.; Tarascon, J.-M. Elucidating the Origin of the Electrochemical Capacity in a Proton-Based Battery HxIrO4 via Advanced Electrogravimetry. *ACS Appl. Mater. Interfaces* **2020**, *12*, 4510–4519. [CrossRef]
45. Gao, W.L.; Sel, O.; Perrot, H. Electrochemical and viscoelastic evolution of dodecyl sulfate-doped polypyrrole films during electrochemical cycling. *Electrochim. Acta* **2017**, *233*, 262–273. [CrossRef]
46. Benmouhoub, C.; Agrisuelas, J.; Benbrahim, N.; Pillier, F.; Gabrielli, C.; Kadri, A.; Pailleret, A.; Perrot, H.; Sel, O. Influence of the Incorporation of CeO_2 Nanoparticles on the Ion Exchange Behavior of Dodecylsulfate Doped Polypyrrole Films: Ac-Electrogravimetry Investigations. *Electrochim. Acta* **2014**, *145*, 270–280. [CrossRef]
47. Levi, M.D.; Salitra, G.; Levy, N.; Aurbach, D.; Maier, J. Application of a quartz-crystal microbalance to measure ionic fluxes in microporous carbons for energy storage. *Nat. Mater.* **2009**, *8*, 872–875. [CrossRef]
48. Sigalov, S.; Levi, M.D.; Salitra, G.; Aurbach, D.; Jänes, A.; Lust, E.; Halalay, I.C. Selective adsorption of multivalent ions into TiC-derived nanoporous carbon. *Carbon* **2012**, *50*, 3957–3960. [CrossRef]
49. Gabrielli, C.; Garcia-Jareño, J.J.; Perrot, H. Charge compensation process in polypyrrole studied by ac electrogravimetry. *Electrochim. Acta* **2001**, *46*, 4095–4103. [CrossRef]
50. Gabrielli, C.; Perrot, H.; Rose, D.; Rubin, A.; Toque, J.P.; Pham, M.C.; Piro, B. New frequency/voltage converters for ac-electrogravimetric measurements based on fast quartz crystal microbalance. *Rev. Sci. Instrum.* **2007**, *78*. [CrossRef]
51. Pan, H.; Li, J.; Feng, Y. Carbon Nanotubes for Supercapacitor. *Nanoscale Res. Lett.* **2010**, *5*, 654. [CrossRef]
52. Pan, H.; Poh, C.K.; Feng, Y.P.; Lin, J. Supercapacitor Electrodes from Tubes-in-Tube Carbon Nanostructures. *Chem. Mater.* **2007**, *19*, 6120–6125. [CrossRef]